ADVANCED MATERIALS
www.advmat.de

Improving Device Efficiency of Polymer/Fullerene Bulk Heterojunction Solar Cells Through Enhanced Crystallinity and Reduced Grain Boundaries Induced by Solvent Additives

*Ming-Shin Su, Chih-Yin Kuo, Mao-Chuan Yuan, U-Ser Jeng, Chun-Jen Su, and Kung-Hwa Wei**

Polymer solar cells based on bulk heterojunction (BHJ) structures, featuring conjugated polymers as donors and fullerene derivatives as acceptors,[1] are being developed for their potential application in the low-cost fabrication of large-area devices. In recent reports, BHJ solar cells incorporating crystalline or low-bandgap conjugated polymers[2] and fullerene derivatives have exhibited maximum power conversion efficiencies (PCEs) of up to 8%.[3] The morphology[4] of the active layer in a BHJ solar cell incorporating a polymer/fullerene thin film plays a critical role affecting the device performance; phase-separated domains in the active layer provide not only interfaces for charge separation of photogenerated excitons but also percolation pathways for charge carrier transport to the respective electrodes, critically affecting the device's PCE. The nanoscale morphology of a polymer/fullerene thin film is greatly affected by (i) the film processing conditions,[5] (ii) the molar ratio (composition) of the polymer and the fullerene,[6] and (iii) the nature of the solvent additive (if any).[7] In particular, BHJ polymer solar cells can exhibit improved device performance after undergoing thermal or solvent annealing or the incorporation of solvent additives, all of which alter the film morphology to a more favorable state relative to that of the as-cast film or the film in the absence of the additive, presumably resulting from (i) self-organization of the polymer units into ordered structures and (ii) appropriate aggregation of fullerene domains to provide percolation networks for charge carrier transport.[6,8] Among these approaches, the addition of solvent additive during the processing of the active layer is the simplest and most effective means of optimizing a BHJ device's morphology; it influences the size of the fullerene domains and enhances the crystallinity of the self-organized polymers by improving the solubility of the fullerenes and slightly elongating the drying time of the active layer. Although chloroform and chlorobenzene provide good solubility for conjugated polymers, they are relatively poor solvents for asymmetric C_{70}-fullerene derivatives such as $PC_{71}BM$; therefore, the need exists for a solvent additive that can bridge the miscibility gap between the conjugated polymer and $PC_{71}BM$ so that more-homogeneous films can be produced. Notably, 1,8-di(*R*)octanes, with different functional groups *R*, can significantly improve the miscibility of $PC_{71}BM$ with the polymer.[7] Moreover, the alkyl chain length of the additive can have a substantial effect on the morphology of the active layer and, therefore, the device's performance.[9] The precise effects of solvent additives on the morphologies of active layers constituted by crystalline polymers and fullerenes are not fully understood because of insufficient structural information extending from the nano- and meso-range.

In this Communication, we demonstrate that the PCE of a device incorporating a PBTTPD/$PC_{71}BM$ (1:1.5, w/w) film as the active layer can be improved from 5% to 7.3% – a relative increase of 45% – after incorporating 1,6-diiodohexane (DIH), an additive of suitable alkyl chain length, during solution processing. We also elucidated the precise active layer morphology with simultaneous synchrotron grazing-incidence small-/wide-angle X-ray scattering (GIWAXS/GIWAXS) and transmission electron microscopy (TEM) and found that the additive DIH not only induced higher polymer crystallinity (2.4 and 3.6 times in the out-of-plane and in-plane directions, respectively), but also decreased the average size of the aggregated fractal-like PC71BM clusters to 30 nm (from 150 nm for the film without additives) by removing their grain boundaries.

Figure 1a presents the molecular structures of poly-{bi(dodecyl)thiophene-thieno[3,4-*c*]pyrrole-4,6-dione} (PBTTPD),[10] {6}-1-(3-(methoxycarbonyl)propyl)-{5}-1-phenyl-[5,6]-C_{71} ($PC_{71}BM$), and the solvent additives DIH, 1,4-diiodobutane (DIB), and 1,8-diiodooctane (DIO), which, along with chloroform (CF), we used to process the active layer. Figure 1b displays the UV–vis absorption spectra of PBTTPD/$PC_{71}BM$ (1:1.5, w/w) films cast with 0.5 vol% of DIB, DIH, and DIO in CF. The intensity of the signal between 400 and 500 nm for the PBTTPD/$PC_{71}BM$ film increased substantially and the peak maximum blue-shifted relative to that of the pristine PBTTPD film because of the additional absorption in this region provided

M.-S. Su, C.-Y. Kuo, M.-C. Yuan, Prof. K.-H. Wei
Department of Materials Science and Engineering
National Chiao Tung University
1001 Ta Hsueh Road, Hsinchu 30050, Taiwan, ROC
E-mail: khwei@mail.nctu.edu.tw
Dr. U.-S. Jeng, Dr. C.-J. Su
National Synchrotron Radiation Research Center
101 Hsin-Ann Road, Science-Based Industrial Park
Hsinchu 30077, Taiwan, ROC

DOI: 10.1002/adma.201101274

ADVANCED MATERIALS
www.advmat.de

www.MaterialsViews.com

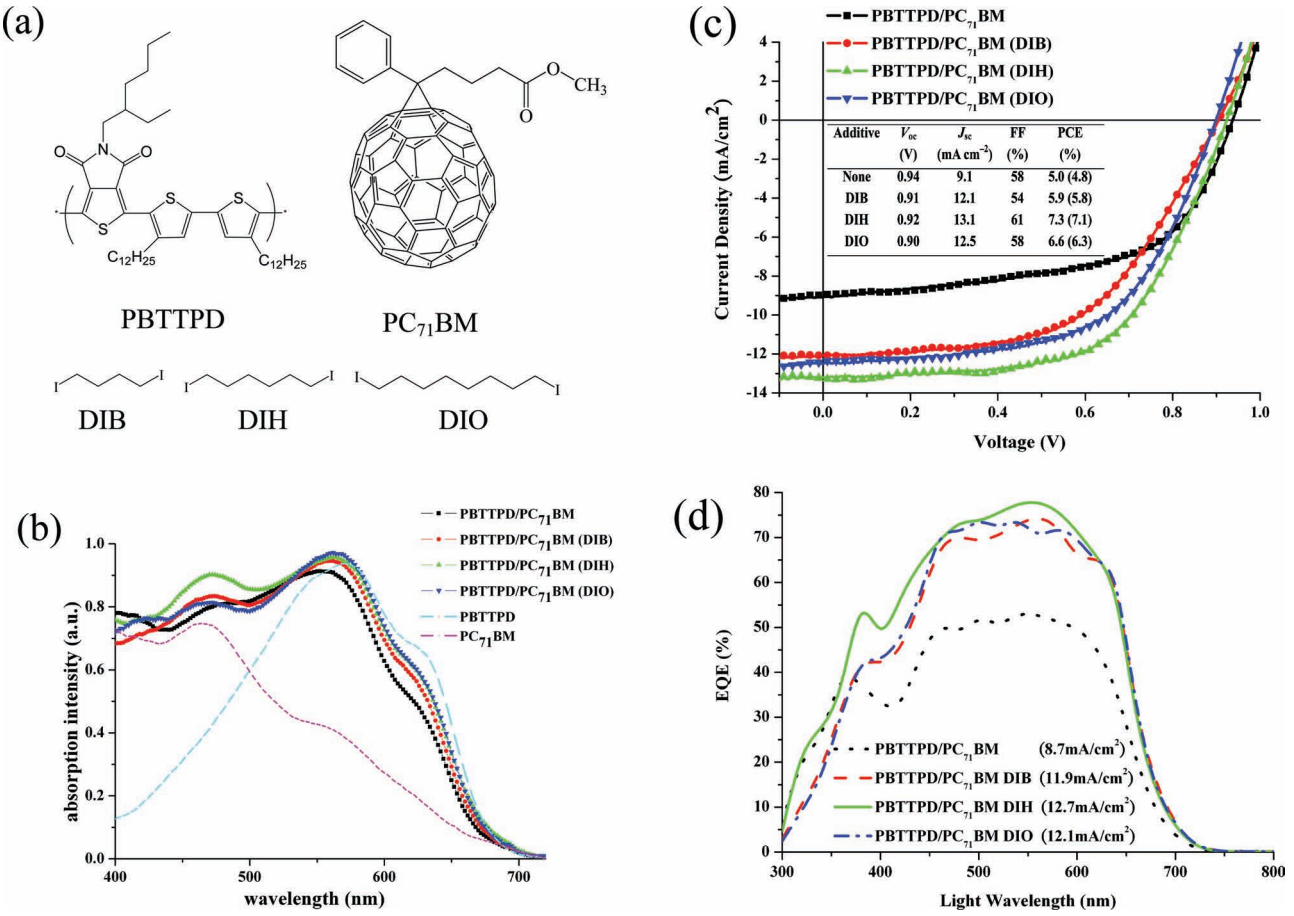

Figure 1. (a) Molecular structures of PBTTPD, $PC_{71}BM$, and the solvent additives DIB, DIH, and DIO. (b) Absorption spectra of PBTTPD/$PC_{71}BM$ films processed from CF (square) and from CF containing 0.5 vol% DIB (circle), DIH (triangle), and DIO (inverted triangle). (c) Current density–voltage curves of PBTTPD/$PC_{71}BM$ devices processed from CF (square) and from CF containing 0.5 vol% DIB (circle), DIH (triangle), and DIO (inverted triangle). The obtained values of V_{oc} and J_{sc} and the FFs and PCEs are listed in the inset table; averaged PCEs are presented in brackets. (d) EQE curves of PBTTPD/$PC_{71}BM$ devices processed from CF (black dashed line) and from CF containing 0.5 vol% DIB (red dotted line), DIH (green line), and DIO (blue dashed/dotted line).

by $PC_{71}BM$ and because the existence of $PC_{71}BM$ disrupted the packing and ordering of PBTTPD. When we incorporated DIB, DIH or DIO as an additive for processing, the UV–vis absorption peak of the resultant PBTTPD/$PC_{71}BM$ films red-shifted slightly, relative to that of the PBTTPD/$PC_{71}BM$ film prepared in the absence of any additives, but retained its vibronic peak at 630 nm. The PBTTPD/$PC_{71}BM$ film processed using DIH displayed slightly higher absorption between 400 and 500 nm than did the PBTTPD/$PC_{71}BM$ films processed with DIB or DIO, presumably because of differences in the degrees of dispersion of $PC_{71}BM$ in PBTTPD.

Figure 1c displays the photovoltaic performances of the devices incorporating PBTTPD/$PC_{71}BM$ films that had been processed with the different solvent additives; the inset lists their open-circuit voltages (V_{oc}), short-current densities (J_{sc}), and fill factors (FF). The open-circuit voltages of the devices featuring PBTTPD/$PC_{71}BM$ active layers were all approximately 0.9 V, regardless of whether they were processed with or without solvent additives. The short-current densities of the devices with PBTTPD/$PC_{71}BM$ active layers that had been processed with the three solvent additives were all greater than 12 mA cm^{-2}, significantly increased from the value of 9 mA cm^{-2} for the PBTTPD/$PC_{71}BM$ active layer that had been processed without any solvent additive. Specifically, the photovoltaic device based on PBTTPD/$PC_{71}BM$ processed with DIH as the solvent additive exhibited the highest short-circuit current density; it was 40% greater than that obtained without solvent additives. Moreover, the FF for the device containing the PBTTPD/$PC_{71}BM$ active layer that had been processed with DIH was the highest among all of these studied devices. As a result, the PCE of the device incorporating the PBTTPD/$PC_{71}BM$ active layer that has been processed with DIH as the solvent additive increased to 7.3% from 5.0% for the corresponding device prepared without any solvent additive. Thus, an optimum chain length exists for the solvent additives' molecular structure to improve the morphology of the active layer and, therefore, device performance.

Figure 1d displays the external quantum efficiencies (EQEs) of the devices containing PBTTPD/$PC_{71}BM$ active layers that had been processed with solvent additives. The PBTTPD/$PC_{71}BM$ devices processed with solvent additives displayed significantly

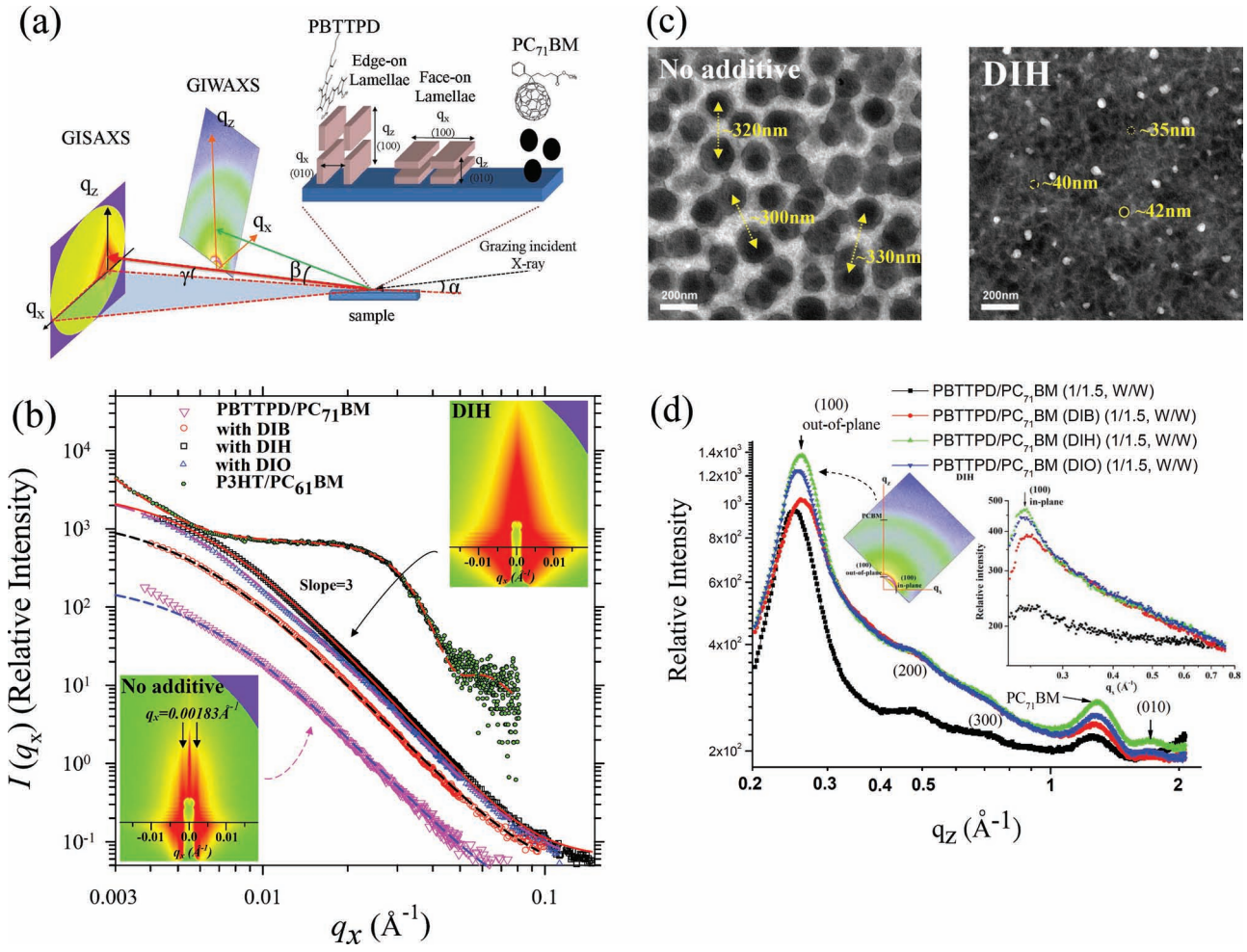

Figure 2. (a) Schematic representation of the GIWAXS and GISAXS set-up; q_z and q_x denote X-ray scattering in the out-of-plane and in-plane directions, respectively. (b) In-plane GISAXS profiles of the PBTTPD/$PC_{71}BM$ films spin-cast in the absence (square) and presence of DIB, DIH or DIO, as indicated. Insets showed GIWAXS patterns of the films processed in the absence and presence of DIH. The data were fitted (dashed or solid curves) using a model of fractal aggregates, as described in the text. The GISAXS spectrum of the P3HT/PCBM film was fitted (dashed curve) using polydisperse spheres. (c) TEM images of PBTTPD/$PC_{71}BM$ films prepared (left) in the absence and (right) presence of the additive DIH. (d) Out-of-plane GIWAXS profiles of the lamellar peaks and the π–π stacking of PBTTPD and the halo of $PC_{71}BM$ aggregation.

enhanced EQEs relative to that for the device with the active layer processed without any solvent additive. The measured short-circuit currents for the devices incorporating PBTTPD/$PC_{71}BM$ active layers processed using DIB, DIH, and DIO were 12.1, 13.1, and 12.5 mA cm^{-2}, respectively; the short-circuit currents obtained from integrating the EQE curves were 11.9, 12.7, and 12.1 mA cm^{-2}, respectively [inset to Figure 1d]; these values are within a 5% error range, indicating the accuracy of our measurements. The fact that the device incorporating the DIH-processed active layer exhibited the highest EQE is consistent with the strong absorption intensity it displays in Figure 1b, implying that it might possess a more favorable active layer morphology.

Figure 2a displays the coordinated GIWAXS and GISAXS set-up that we used to simultaneously deduce the orientation and crystallinity of the PBTTPD crystal lamellae and the aggregation of $PC_{71}BM$ on length scales of up to a few tens of nanometers, respectively, in the thin films; this setup can behave as a precise and statistically meaningful probe of the different phases present in the same spot. Figure 2b presents GISAXS profiles recorded along the in-plane direction, q_x, of the 2D images for ca. 90-nm-thick PBTTPD/$PC_{71}BM$ (1:1.5, w/w) films that had the same composition as those used in the active layers of the devices. The scattering intensity in the in-plane direction, $I(q_x)$, for the PBTTPD/$PC_{71}BM$ films processed with or without additives exhibited the same power-law scattering behavior with respect to the in-plane wavevector q_x [i.e., $I(q_x) \mu q_x^{-D}$], with the fractal dimension D of approximately 3 (in the region of q_x greater than ca. 0.01 $Å^{-1}$) indicating a fractal-like (porous) $PC_{71}BM$ aggregate. Notably, the values of $I(q_x)$ similarly measured for the P3HT/$PC_{61}BM$ (1:1, w/w) film after thermal annealing (150 °C, 15 min) revealed characteristically different scattering behavior in the q_x region > 0.01 $Å^{-1}$, due to denser packing of the $PC_{61}BM$ aggregates. Additionally, the inset in the lower-left-hand corner of Figure 2(b) displays a corresponding 2D GISAXS pattern, with strong interference peaks at a value of q_x of 0.00183 $Å^{-1}$, revealing a large mean

spacing of 343 nm formed by a monolayer of aggregated clusters in the in-plane direction of the film. In contrast, the inset in the upper-right-hand corner of Figure 2(b) reveals no such interference peaks for the PBTTPD/$PC_{71}BM$ film prepared with DIH as the additive. Moreover, the power law scattering behavior for the scattering intensity in the in-plane direction of the PBTTPD/$PC_{71}BM$ films processed with the additives fades out in this low-q_x region (<0.007 $Å^{-1}$), implying a cluster size of a few tens of nanometers. To characterize the $PC_{71}BM$ fractal clustering size, 2ξ, we fitted the $I(q_x)$ data from the PBTTPD/$PC_{71}BM$ films processed with or without additives using a fractal model (see the Supporting Information) and a universal fractal dimension D of approximately 3. The fitted $PC_{71}BM$ fractal cluster sizes (2ξ) for the PBTTPD/$PC_{71}BM$ films processed without any additive and with DIB, DIH, and DIO were 40, 36, 32, and 39 nm, respectively.

From the GISAXS analysis, we conclude that the active layers processed with the additives featured smaller and better-dispersed $PC_{71}BM$ domains and, therefore, formed better network morphologies than that the film cast without any solvent additives. Among the tested additives, DIH provided the finest dispersion of $PC_{71}BM$, presumably because it optimized the balance between the solubility of $PC_{71}BM$ and the interactions between the additive and the polymer molecules. Figure 2(c) displays TEM images of PBTTPD/$PC_{71}BM$ (1:1.5, w/w) films cast with and without the additive DIH; the bright and dark regions correspond to PBTTPD- and PCBM-rich domains, respectively, because the differences in the electron scattering densities of fullerenes (1.5 g cm^{-3}) and polymers (1.1 g cm^{-3}) are quite large. Large $PC_{71}BM$ grains (size: ca. 150 nm; mean spacing: ca. 340 nm) are evident in the image of the film processed without any additive while the size of $PC_{71}BM$ grains reduced to ca. 30 nm for the PBTTPD/$PC_{71}BM$ film prepared with DIH as the additive. These morphological differences induced by the additives in the mesoscale are consistent with our GISAXS results; the internal structures of the 150-nm grains (consisting

Table 1. Structure parameters for PBTTPD/$PC_{71}BM$ films processed with and without additives; 2ξ is the size of the fractal clusters of $PC_{71}BM$; χ and L are the relative crystallinity and edge-on (or face-on) lamellar size, respectively, of the conjugate polymer.

Additive	2ξ (nm) ($PC_{71}BM$)	χ (%) (edge-on lamellae) (100) out-of-plane	L (nm) (edge-on lamellae) (100) out-of-plane	χ (%) (face-on lamellae) (100) in-plane	L (nm) (face-on lamellae) (100) in-plane
None	40 ± 2	21	31	3	3
DIB	36 ± 1	26	24	9	11
DIH	32 ± 1	49	24	11	13
DIO	39 ± 1	41	24	10	13

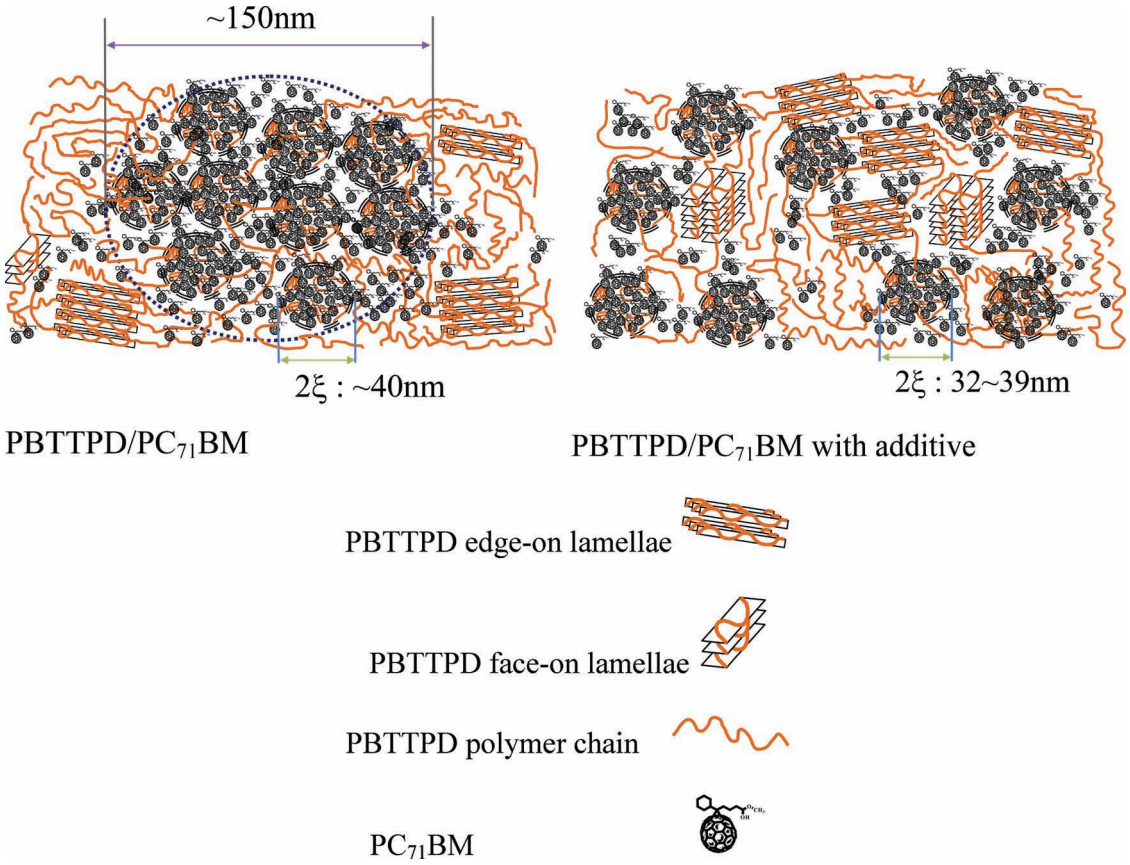

Figure 3. Schematic representations of mesograins in PBTTPD/$PC_{71}BM$ films processed in the (left) absence and (right) presence of an additive. In the presence of the additive, the mesoscale grains dissolved into smaller fractal clusters; the additive also intercalated with the PBTTPD lamellar nanodomains. The fractal-like $P_{71}CBM$ clusters were circular objects filled with interconnected $PC_{71}BM$ units.

of 40-nm clusters), respectively in the PBTTPD/$PC_{71}BM$ films processed without any additive.

Figure 2d presents the detailed out-of-plane and in-plane direction intensities of the PBTTPD/$PC_{71}BM$ (1:1.5, w/w) films processed with and without additives. The strong out-of-plane (100) peak at a value of q_z of 0.24 $Å^{-1}$ is due to edge-on PBTTPD lamellae; the amorphous halo centered at a value of q_z of 1.26 $Å^{-1}$ corresponds to short-range ordering caused by the $PC_{71}BM$ aggregates in the PBTTPD/$PC_{71}BM$ films. One additional characteristic peak was present for the PBTTPD/$PC_{71}BM$ films that had been processed with DIB, DIH, and DIO as additive: an out-of-plane (010) signal at a value of q_z of 1.7 $Å^{-1}$. This weak signal resulted from face-on PBTTPD lamellae or from π–π stacking of the PBTTPD units; these face-on lamellae would also result in an in-plane (100) peak at a value of q_x of ca. 0.24 $Å^{-1}$. The inset to Figure 2d reveals that the intensities of the in-plane (100) peaks at a value of q_x of ca. 0.24 $Å^{-1}$ for the PBTTPD/$PC_{71}BM$ films processed with the additives were enhanced relative to that of the film processed without any additives, with the largest increase in the case of DIH as the additive. **Table 1** summarizes the corresponding lamellar spacings and sizes estimated from the Scherrer equation and the relative crystallinities from the integrated intensities of the (100) peaks for the edge-on and face-on PBTTPD lamellae. The introduction of the additives during processing enhanced the crystallinity of both the edge-on and face-on PBTTPD lamellae, with slightly reduced edge-on lamellar sizes and increased face-on lamellar sizes. The PBTTPD/$PC_{71}BM$ film processed with DIH as the additive displayed higher crystallinity—2.4 times and 3.6 times for the PBTTPD edge-on lamellae and face-on lamellae, respectively—as large as that of the PBTTPD/$PC_{71}BM$ film that had been cast without any additive. Therefore, DIH provided superior results, compared with DIB and DIO, when used as the additive for the PBTTPD/$PC_{71}BM$ film. Nevertheless, the optimized chain length of this diiodoalkane might not necessarily be appropriate for other homologous systems; the polarity of the additive, with respect to the specific conjugate copolymer and $PC_{71}BM$, must be taken into consideration.

Figure 3 presents schematic representations of the PBTTPD/$PC_{71}BM$ morphologies that are consistent with the structural information obtained from the GISAXS, GIWAXS, and TEM analyses. These drawings depict the additive not only inducing higher polymer crystallinity in both the out-of-plane and in-plane directions but also removing the grain boundary of the aggregated fractal-like $PC_{71}BM$ clusters, leading to superior pathways for carrier transport.

In conclusion, we have fabricated a BHJ solar cell device incorporating a PBTTPD/$PC_{71}BM$ thin film that exhibited a PCE of 7.3% when the active layer was processed with DIH, a diiodoalkane additive, which effectively induced higher polymer crystallinity and removed the grain boundary of the large $PC_{71}BM$-rich grains, resulting in a more-uniform film morphology on the mesoscale.

Supporting Information

Supporting Information is available from the Wiley Online Library or from the author.

Acknowledgements

We thank the National Science Council for financial support (NSC 99–2120-M009–003).

Received: April 5, 2011
Revised: May 6, 2011
Published online: June 14, 2011

[1] G. Yu, J. Gao, J. C. Hummelen, F. Wudl, A. J. Heeger, *Science* **1995**, *270*, 1789.

[2] a) H. Y. Chen, J. Hou, S. Zhang, Y. Liang, G. Yang, Y. Yang, L. Yu, Y. Wu, G. Li, *Nat. Photon.* **2009**, *3*, 649; b) Y. Liang, Y. Wu, D. Feng, S. T. Tsai, H. J. Son, G. Li, L. Yu, *J. Am. Chem. Soc.* **2009**, *131*, 56; c) S. H. Park, A. Roy, S. Beaupre, S. Cho, N. Coates, J. S. Moon, D. Moses, M. Leclerc, K. Lee, A. J. Heeger, *Nat. Photon.* **2009**, *3*, 297; d) F. Huang, K. S. Chen, H. L. Yip, S. K. Hau, O. Acton, Y. Zhang, J. Luo, A. K. Y. Jen, *J. Am. Chem. Soc.* **2009**, *131*, 13886; e) C. V. Hoven, X. D. Dang, R. C. Coffin, J. Peet, T. Q. Nguyen, G. C. Bazan, *Adv. Mater.* **2010**, *22*, E63; f) C. Piliego, T. W. Holcombe, J. D. Douglas, C. H. Woo, P. M. Beaujuge, J. M. J. Fréchet, *J. Am. Chem. Soc.* **2010**, *132*, 7595; g) Y. Zhang, S. K. Hau, H. L. Yip, Y. Sun, O. Acton, A. K.-Y. Jen, *Chem. Mater.* **2010**, *22*, 2696; h) T. Y. Chu, J. Lu, S. Beaupré, Y. Zhang, J. R. Pouliot, S. Wakim, J. Zhou, M. Leclerc, Z. Li, J. Ding, Y. Tao, *J. Am. Chem. Soc.* **2011**, *133*, 4250; i) G. Y. Chen, Y. H. Cheng, Y. J. Chou, M. S. Su, C. M. Chen, K. H. Wei, *Chem. Comm.* DOI: 10.1039/c1cc10585j.

[3] M. A. Green, K. Emery, Y. Hishikawa, W. Warta, *Prog. Photovolt: Res. Appl.* **2011**, *19*, 84.

[4] a) H. Sirringhaus, P. J. Brown, R. H. Friend, M. M. Nielsen, K. Bechgaard, B. M. W. Langeveld-Voss, A. J. H. Spiering, R. A. J. Janssen, E. W. Meijer, P. Herwig, D. M. de Leeuw, *Nature* **1999**, *401*, 685; b) M. C. Quiles, T. Ferenczi, T. Agostinelli, P. G. Etchegoin, Y. Kim, T. D. Anthopoulos, P. N. Stavrinou, D. D. C. Bradley, J. Nelson, *Nat. Mater.* **2008**, *7*, 158; c) H. Ma, H. L. Yip, F. Huang, A. K.-Y. Jen, *Adv. Funct. Mater.* **2010**, *20*, 1371.

[5] a) G. Li, Y. Yao, H. Yang, V. Shrotriya, G. Yang, Y. Yang, *Adv. Funct. Mater.* **2007**, *17*, 1636; b) F. Padinger, R. S. Rittberger, N. S. Sariciftci, *Adv. Funct. Mater.* **2003**, *13*, 85; c) R. Hamilton, C. G. Shuttle, B. O'Regan, T. C. Hammant, J. Nelson, J. R. Durrant, *J. Phys. Chem. Lett.* **2010**, *1*, 1432; d) L. M. Chen, Z. Xu, Z. Hong, Y. Yang, *J. Mater. Chem.* **2010**, *20*, 2575.

[6] a) M. Y. Chiu, U. Jeng, M. S. Su, K. H. Wei, *Macromolecules* **2010**, *43*, 428; b) S. S. van Bavel, M. Barenklau, G. de With, H. Hoppe, J. Loos, *Adv. Funct. Mater.* **2010**, *20*, 1458; c) A. C. Mayer, M. F. Tony, S. R. Scully, J. Rivnay, C. J. Brabec, M. Scharber, M. Koppe, M. Heeney, I. McCulloch, M. D. McGehee, *Adv. Funct. Mater.* **2009**, *19*, 1173.

[7] a) J. K. Lee, W. L. Ma, C. J. Brabec, J. Yuen, J. S. Moon, J. Y. Kim, K. Lee, G. C. Bazan, A. J. Heeger, *J. Am. Chem. Soc.* **2008**, *130*, 3619; b) J. M. Szarko, J. Guo, Y. Liang, B. Lee, B. S. Rolczynski, J. Strzalka, T. Xu, S. Loser, T. J. Marks, L. Yu, L. X. Chen, *Adv. Mater.* **2010**, *22*, 5468; c) J. T. Rogers, K. Schmidt, M. F. Toney, E. J. Kramer, G. C. Bazan, *Adv. Mater.* DOI: 10.1002/adma.201003690; d) M. S. Su, H. C. Su, C. Y. Kuo, Y. R. Zhou, K. H. Wei, *J. Mater. Chem.* **2011**, *21*, 6217.

[8] M. Y. Chiu, U. Jeng, C. H. Su, K. S. Liang, K. H. Wei, *Adv. Mater.* **2008**, *20*, 2573.

[9] J. Peet, J. Y. Kim, N. E. Coates, W. L. Ma, D. Moses, A. J. Heeger, G. C. Bazan, *Nat. Mater.* **2007**, *6*, 497.

[10] M. C. Yuan, M. Y. Chiu, S. P. Liu, C. M. Chen, K. H. Wei, *Macromolecules* **2010**, *43*, 6936.